Colloid Polym Sci 276:577–588 (1998)

ORIGINAL CONTRIBUTION

W. Schrof
J. Klingler
W. Heckmann
D. Horn

Confocal fluorescence and Raman microscopy in industrial research

Received: 5 February 1998
Accepted: 16 February 1998

Dedicated to Prof. Dr. hc Milan Schwuger on the occasion of his 60th birthday

W. Schorf (✉) · J. Klinger
W. Heckmann · D. Horn
BASF AG
Polymers Laboratory
D-67056 Ludwigshafen
Germany

Abstract Modern chemical and pharmaceutical industrial research benefits from improved spectroscopic tools. New developments in confocal fluorescence and Raman microscopy lead to an increase in sensitivity, selectivity and speed of microscopic imaging and fluctuation analysis resulting in a better understanding of structure–property relationships essential for targeted development.

In this paper we report on the application of fluorescence and Raman microscopy for characterizing the morphology of polymeric multiphase solid-state samples and on new developments in the corresponding correlation spectroscopies for the characterization of the dynamics of complex colloidal systems in the liquid state. In the case of fluorescence new technological opportunities are gained by two-photon excitation.

Key words Confocal microscopy – confocal Raman microscopy – chemical imaging – laser scanning confocal microscopy – two-photon-microscopy – fluorescence correlation spectroscopy – Raman correlation spectroscopy

Introduction

Targeted development work in chemical and pharmaceutical industrial research, in general, benefits greatly from the rapid advances in analytical instrumentation in fluorescence and Raman microscopy and spectroscopy [1]. In this paper we will concentrate on new developments in the application of fluorescence and Raman microscopy and spectroscopy of multiphase polymeric materials as well as fluorescence and Raman correlation spectroscopy to characterize biological and polymeric colloidal systems in the liquid phase. Fluorescence techniques yield sensitivity, selectivity and speed [2, 3], Raman spectroscopy allows chemical identification [4], whereas confocal optical microscopy [5, 6] gives a spatial resolution of about 1 μm^3 without complicated sample preparation procedures.

The rapid progress in these areas of instrumentation is mainly driven by recent developments in the field of laser, filter, detector and computer technology [7].

Turn-key all-solid-state laser systems [8] revolutionize the light sources needed for microspectroscopy. Semiconductor laser diodes boost the laser efficiency and minimize energy, cooling water and space consumption [9]. As a consequence, intense cw or pulsed laser operation is available at different wavelengths in the UV, visible and near-infrared (NIR) spectral range from small frame lasers. Nonlinear optical effects like frequency doubling and mixing [10] lead to tailor-made wavelengths ranging from the NIR to UV spectral regime. Further, laser radiation can be guided by optical fibers [11] without complicated mirror arrangements thus greatly enhancing the potential of in situ applications even in hazardous environments.

Lasers with single axial mode operation help to achieve far-field focus diameters only limited by diffraction [7]. The high laser intensity compensates for the small measuring volume and allows to use low cross-section effects like Raman scattering as analytical tools.

The invention of steep edge or bandpass filters (notch filters) result in small effective spectral filtering elements [12] without low-throughput double or triple monochromators.

New detector technologies like the multichannel Si-CCD chip (Charge Coupled Device) [13] or the Si avalanche photodiode [14] with very high quantum yields in a broad spectral range from 400 to 1000 nm improve the measuring sensitivity [7]. New miniaturized photomultiplier modules and arrays with integrated power supplies manifest the progress in the traditional detector techniques [15]. All these techniques benefit from sophisticated electronics for readout and computer programs for filtering, noise reduction and image analysis to reduce the flood of measuring data to the relevant parameters.

Confocal microscopy

The principal optical setup of a confocal microscope [5, 6] is given in Fig. 1. The excitation beam is spatially filtered by a telescope including an illumination pinhole to maintain a Gaussian beam profile. In the case of a laser with a single axial mode profile or by using a single-mode excitation fiber, this procedure can be omitted. The microscope objective focuses the laser beam onto the sample. The emitted fluorescence or inelastically scattered Raman light is collected by the same microscope objective, passed through a dichroic mirror and focused onto an aperture placed in the confocal plane. Only light from the laser focus can pass the confocal aperture. Light from other sample regions, e.g. other depth layers, is efficiently blocked. Laser light in the detection path is eliminated by the dichroic mirror followed by an edge or bandpass filter or a spectrograph in front of the detector. The diameter of the confocal aperture mainly determines the confocal detection volume. To minimize the illumination spot, a high-aperture microscope, and a beam diameter fitting to the optical width of the objective should be used. A careful alignment of the confocal aperture in all three spatial dimensions to fit the confocal spot is needed to confine the minimal measuring volume while maintaining the maximum detector signal.

In the case of fluorescence, the confocal aperture and its precise alignment can be avoided by using two-photon excitation, where the three-dimensional measuring volume is defined by the excitation conditions only. The effect of

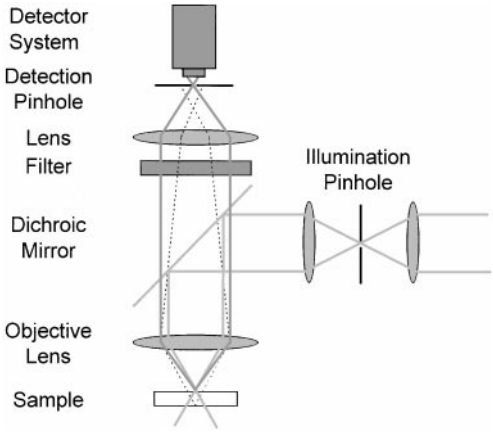

Fig. 1 Confocal microscopy by confocal aperture detection, radiation out of the focus (full line) can pass the detection pinhole, radiation from other regions (dashed line) is blocked

two-photon excitation [7, 10] is based on the nonlinear extension of the simple Lambert–Beer's law of absorption. The absorption coefficient can be approximated by the constant term well known from linear optics and an additional intensity-dependent part. Focusing of ultrashort laser pulses e.g. from modelocked Ti–sapphire lasers can yield light intensities high enough to induce this nonlinear absorption at wavelengths where one-photon excitation is forbidden. As shown in Fig. 2, two photons will be absorbed simultaneously. The energy of the two photons must be sufficient to reach the excited electronic state.

Adjusting the peak power of the laser properly will result in a nonvanishing two-photon absorption only in the laser focus itself. Outside the two-photon absorption probability i.e. the density of excited states will drop exponentially. Thus, the lateral confinement will be caused by the microscope objective while the depth confinement is due to the intensity dependence of two-photon absorption (see Fig. 2b and c). The drawback of using a more expensive pulsed laser can sometimes be compensated by several factors: (1) one can use very simple optics, lenses instead of microscope objectives, and detectors with large sensitive areas which can be simply aligned. (2) sensitive samples like proteins will be excited only in the laser focus and not in a cone of the impinging laser light [16].

The principle of two-photon confinement of the measuring volume is in a reduced way also applicable to Raman spectroscopy by the effect of hyper Raman scattering, if no excited states are generated leading to unwanted heat dissipation or fluorescence emission. The linewidth of the pulsed laser has to be controlled, too. Otherwise the Raman bands will be smeared out.

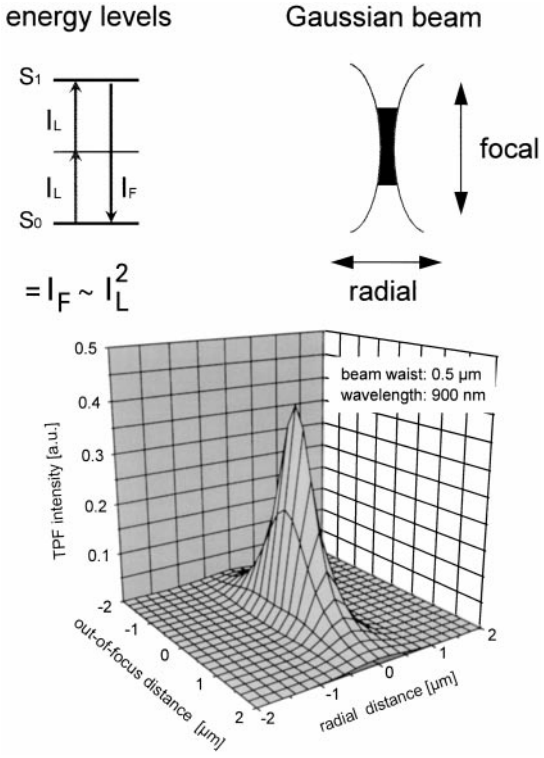

Fig. 2 Confocal fluorescence microscopy by two-photon excitation, (top left) energy level diagram showing the two-photon transition from ground state S_0 to the excited state S_1 via a virtual level, the simultaneous absorption of two red photons can cause a blue fluorescence, (top right) three-dimensional confinement of two-photon excitation. Only in the focus of the Gaussian beam the two-photon absorption and hence fluorescence is possible, (bottom) intensity of the two-photon fluorescence as a function of the radial and longitudinal distance from the focus

Illustrative examples of confocal microscopy

Imaging

Confocal laser scanning fluorescence microscopy of polymer blends

Multihollow micron-sized latex particles from self-emulsifying polymer blends

Hard latex particles with interior cavities are useful as opacifiers for paints and paper coatings. Visible light is scattered most efficiently by voids having diameters in the range of 200–800 nm. The preparation of such micron-sized latex particles is described elsewhere [17] in more detail. It is based on polymer blends that are self-emulsifying in water, forming secondary dispersions.

To find out whether the interior cavities are formed by the aqueous or the organic phase, the aqueous phase was stained by the addition of the water soluble fluorescence dye fluorescein. After removal of the organic solvents, the resulting dispersion was observed by a laser scan microscope operating in the fluorescence mode. Excitation was achieved by irradiation with blue light (488 nm) and on the emission side a longpass filter was used.

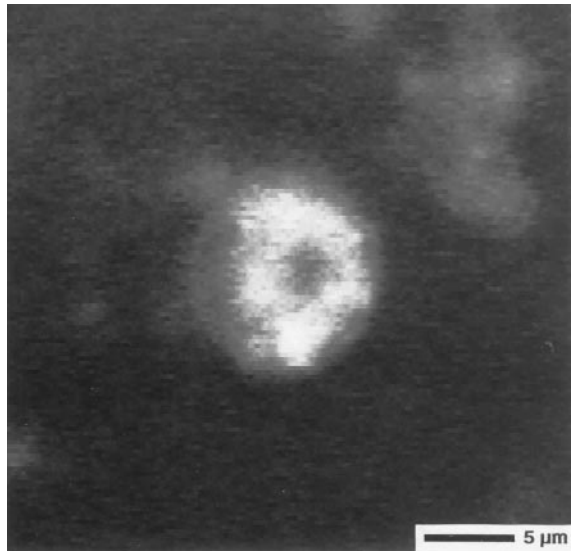

Fig. 3 Visualization of the aqueous cavities in a multihollow particle by confocal fluorescence microscopy

In Fig. 3 an optical section through a single multihollow particle is shown. Fluorescent light is emitted from the interior cavities with high intensity. This is taken as a proof that the cavities contain the aqueous phase.

Modification of asphalt by polymer latex dispersions

Polymer dispersions on the basis of polybutadiene copolymers, block copolymers and other elastomers are added to classical road asphalt in order to improve permanent deformation occuring at high temperatures (rutting), load-associated fatigue cracking and low-temperature thermal cracking [18]. Such blends are generally multiphase systems. The way these components are distributed in the asphalt influences the mechanical properties. It is believed that an interconnecting network of polymer modifier is responsible for good mechanical performance.

By far the most valuable method to characterize structure and homogeneity of polymer-modified asphalt is fluorescence microscopy, because intrinsic aromatic fluorescent constituents in the asphalt are soaked into the polymers thus selectively marking them. In Fig. 4, the morphology of an asphalt/polymer-blend is shown. A polymer dispersion was used for modification. The latex particles are agglomerated and form a fibrillar network

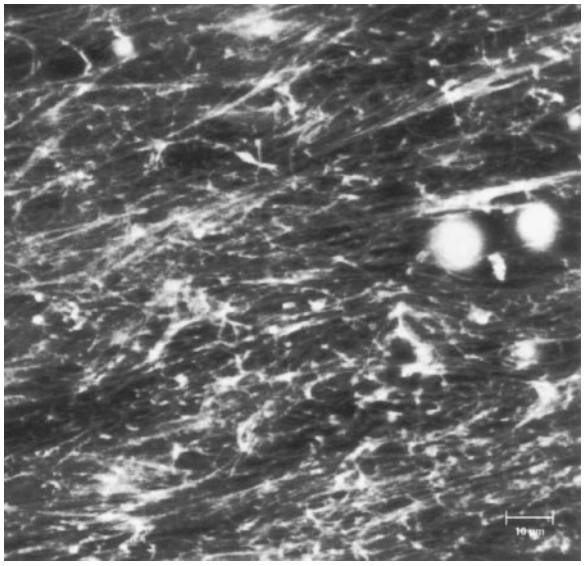

Fig. 4 Confocal fluorescence micrograph of polymer fibrils in asphalt modified with a dispersion based on polybutadiene copolymer. The fibrils are oriented due to melt flow

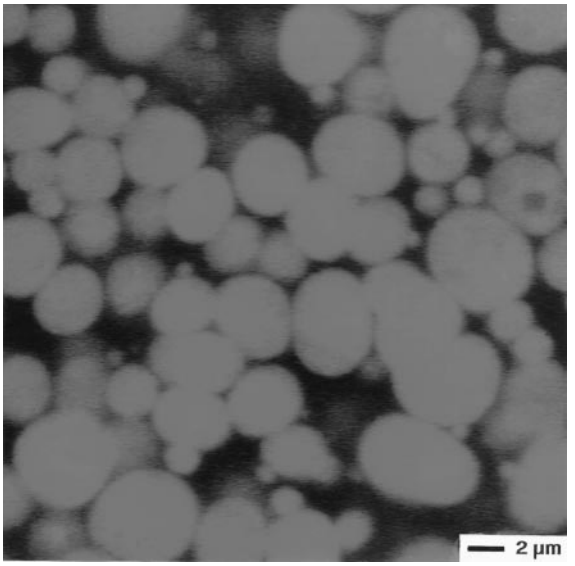

Fig. 5 Optical section through a polyamide/poly(phenylene ether)-blend. The fluorescent bright PPE-particles are dispersed in the PA-matrix

throughout the sample. Due to the melt flow the fibrils are oriented.

Morphology of a polyamide/poly(phenylene ether)-blend

Fluorescence microscopy can also be used to characterize polymer blend morphologies if one of the polymer components shows sufficient fluorescence and if the polymer phases are large enough to be imaged in a light microscope. As an example, Fig. 5 shows an optical section through a polyamide/poly(phenylene ether)-blend (PA/PPE). The fluorescing PPE-particles are imaged bright (red due to the special look up table) against the dark PA-matrix. The PPE-particles also contain a block copolymer as an impact modifier which cannot be resolved. To image the impact modifier it would be necessary to obtain transmission electron micrographs.

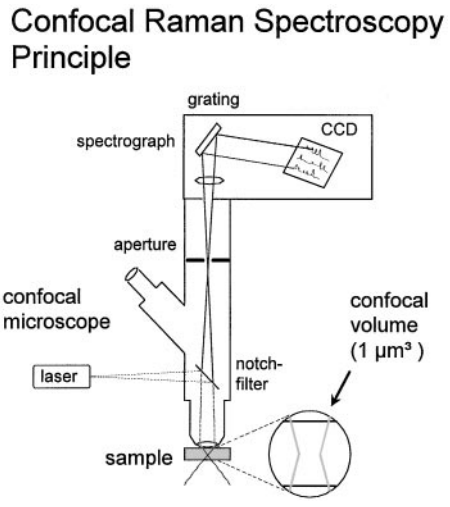

Fig. 6 Schematic layout of confocal Raman microscope

Confocal Raman microscopy of multicomponent polymeric systems

Confocal Raman spectroscopy combines the chemical information from vibrational spectroscopy with the spatial resolution of confocal microscopy [4, 19–21]. A typical optical setup of a Raman microscope is given in Fig. 6. With such an instrument Raman spectra from a confined measuring volume as small as 1 μm^3 can be detected in backscattering geometry. A number of technical improvements in modern Raman spectrometers result in short measuring times with small confocal volumes, despite the small Raman cross section: notch filters to selectively suppress laser Rayleigh scattering while transmitting Raman photons, high throughput single grating spectrographs and sensitive low-noise cooled CCD arrays for parallel detection of all Raman bands. The depth profiles or lateral Raman mappings can be recorded by moving the sample through the focus of the microscope objective by a *xyz* translational stage.

Depth profiling of radiation-cured polymers

The process of radiation curing converts an easily coatable low-viscosity formulation of reactive prepolymers,

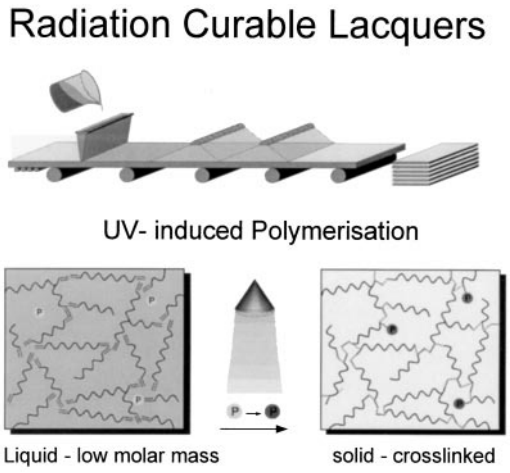

Fig. 7 UV curing of acrylic coatings formulations

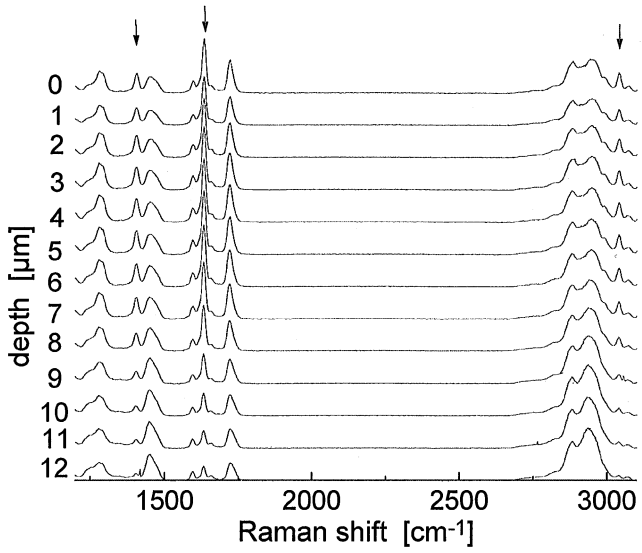

Fig. 8 Depth profile of cured polyetheracrylate, the reactive acrylate groups are marked by arrows

oligomers, monomers, photoinitiators and additives into a protective solid-state coating within fractions of seconds just by illumination with UV light or an electron beam [22–24] (see Fig. 7). Fields of application are the surface refinement of furniture, wooden floor coverings, paper, metals, polymers, etc. Benefits are high speed, low investment and energy costs, low concentrations of extractables, no need to handle organic solvents.

This technological advantage, however, simultaneously bears the disadvantage, that the reacted polymer as a crosslinked structure withstands every classical polymer characterization and classification. We will demonstrate how confocal Raman microscopy can characterize these solid three-dimensionally crosslinked films by spatially mapping the reaction conversion or the distribution of additives [25]. The coating formulations are doctor-bladed onto glass substrates and UV cured. The films can then be investigated in the Raman microscope without further sample preparations. In the case of limited optical penetration – as with pigmented coatings – thin sections can be prepared by microtomy. Thus depth profiling can be transformed to lateral mapping.

Depth profiling to investigate oxygen inhibition

One possible problem of UV curing of acrylic formulations is that the surface of the coating layer stays tacky while the bulk is fully hardened. Such an inhibition of the radical curing reaction is caused by the reaction of photoinitiator radicals and polymer radicals with dissolved and penetrating oxygen.

$$R_\bullet + O_2 \rightarrow R\text{–}O\text{–}O_\bullet$$

$R_\bullet$ = photoinitiator or polymer radical.

The hydroperoxide radicals formed by this reaction are relatively stable and no longer active for polymerization. Thus, the polymerization will be inhibited or slowed to a point, where no progress of the reaction will be found. Figure 8 shows depth-resolved Raman spectra for a UV-cured polyetheracrylate formulation. The progress of the radical curing reaction is monitored by the consumption of carbon double bonds, the Raman bands of which are marked by arrows. Unreacted acrylate bands are found in a surface layer of about 7 μm, whereas they vanish in deeper layers. In Fig. 9 the reaction conversion is plotted for the polyetheracrylate of Fig. 8 and for two modified formulations, one containing an amine synergist, the other a paraffine surface additive. The high surface curing of the modified formulations is a result of the oxygen deactivation of the amine and of a paraffine surface barrier preventing oxygen penetration into the coating layer, respectively. This example shows the confocal Raman spectroscopy is well suited to investigate oxygen inhibition near the surface of coatings. The destruction-free analytical tool helps the chemist to circumvent unwanted solid-state reactions in selected parts of the samples. In case of oxygen inhibition successful technical measures are: Increased intensities of irradiation, curing under inert atmosphere or under protective foils, or higher concentration of photoinitiators [22].

Imaging of glass fiber reinforced, flame retardant polyamide extrudates

Another strength of confocal Raman microscopy is the ability to monitor the distribution of different ingredients

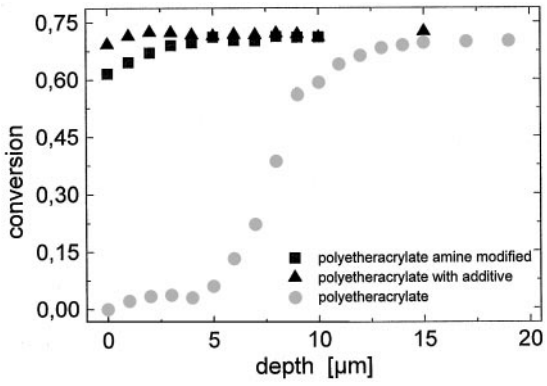

Fig. 9 Depth profile of conversion of different polyetheracrylates

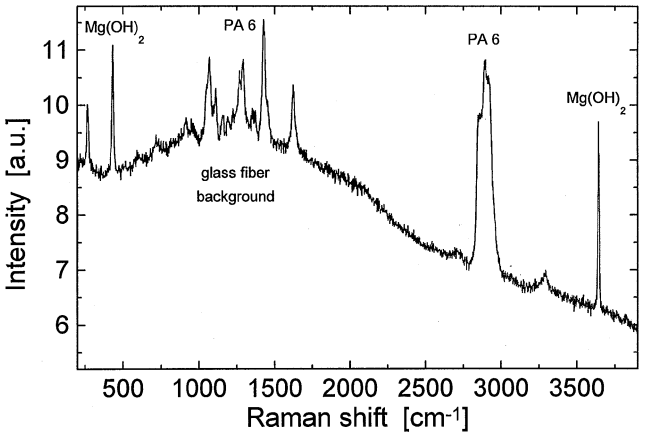

Fig. 10 Raman spectrum of glass fiber reinforced, flame-retardent polyamide extrudate

of a formulation. Such a Raman mapping can give proof of homogeneous or inhomogeneous mixtures without additional staining or other complicated sample preparations. Material problems e.g. mechanical rupture can be predicted from measurements on a microscopic scale.

A typical example for a multicomponent polymer system are extruded polyamide plates equipped with $Mg(OH)_2$ as flame retardants [26] and glass fiber reinforcement. At the higher temperatures occurring in incineration processes $Mg(OH)_2$ will release water thus acting as a flame retardant. Glass fibers are commonly used to improve mechanical properties. The Raman spectrum of this composite is plotted in Fig. 10. The inorganic flame retardant shows sharp peaks at very low and very high wave numbers, whereas Raman bands of the polyamide are found in the fingerprint range and around 3000 cm^{-1} (CH– and NH vibrations). The glass fibers yield a very broad fluorescence background. In this case, the well-established procedure to clean Raman spectra by background subtraction would result in destruction of valuable information.

The local distribution of the ingredients of our extrudate is determined by Raman mapping (see Figs. 11 and 12). An area of $90 \times 90\,\mu m^2$ is analyzed with a spatial resolution of $3\,\mu m$ in this case. In our example the local ratio of polyamide vs $Mg(OH)_2$ concentration is statistically fluctuating by a factor as high as 3 (Fig. 11). By contrasting the fluorescent background the distribution of glass fiber is found (Fig. 12). One fiber lies parallel to the surface and two others directly into the bulk.

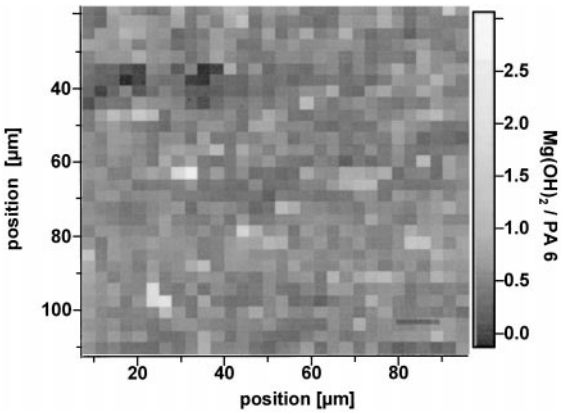

Fig. 11 Mapping of glass fiber reinforced, flame-retardent polyamide extrudate. Ratio of flame retardent $Mg(OH)_2$ vs. polyamide

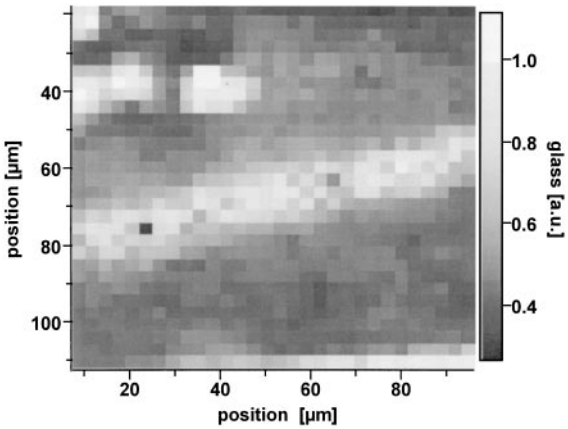

Fig. 12 Mapping of glass fiber reinforced, flame-retardent polyamide extrudate. Glass fibers are contrasted by their fluorescence background

Number fluctuation analysis by correlation spectroscopy

Fluorescence correlation spectroscopy (FCS) [27–29] and its vibrational spectroscopic counterpart Raman correlation spectroscopy (RCS) [30] are analytical tools using

number fluctuations of fluorescent or Raman active molecules (or particles) in the very small confocal observation volume to obtain information on the dynamic properties of these molecules or particles.

Fluorescence correlation spectroscopy

The experimental setup for FCS is very similar to Fig. 1 [31]. The light of a laser is coupled into a single-mode optical fiber and passes through the illumination pinhole onto a dichroic mirror. The reflected light is focused by a microscope objective. The fluorescence excited in the sample is collected by the objective and focused through the mirror and the detection pinhole onto a detector. The electric signal of this detector is fed into a hardware correlator, where an autocorrelation function (ACF) of the observed fluorescence intensity fluctuations is calculated. The observed intensity fluctuations are caused by Brownian motion leading to number fluctuations in the observation volume. For an idealized experiment, the resulting ACF is given by [32]

$$G(t) = 1 + \frac{1}{N}\left[\frac{1}{1 + (4Dt/r^2)}\right],$$

where N is the average number of fluorescent molecules in the observation volume, D their thermal diffusion coefficient and r the radial width of the observation volume. The diffusion coefficient can be converted to a hydrodynamic diameter by the Stokes–Einstein equation

$$d = \frac{k\,T}{3\pi\eta D},$$

where d is the hydrodynamic diameter of the molecule, k the Boltzmann constant, T the absolute temperature and η the viscosity of the medium.

Because of the fluorescence quantum yields and the integral fluorescence detection, FCS can reach single-molecule detection sensitivity. Experiments were reported with an average number of 10^{-2} molecules in the confocal measuring volume [32]. The high sensitivity and the spectral selectivity of FCS, namely, the ability to derive diffusion coefficients of a very low concentration of fluorescent molecules in a complex system, makes FCS an interesting technique for biophysics [29, 32] and colloid chemistry [33]. For systems that show no intrinsic fluorescence, one has to either label one of the components by covalent binding of a fluorophore or introduce a fluorescent probe into the system, that specifically associates with the component of interest.

Fluorescence correlation spectroscopy (FCS) to study complexation of biological systems: Thrombin–Thrombin inhibitor

Discovery of new lead structure for drugs involves brute-force testing of a huge number of compounds, originating from classical synthesis or synthesized by combinatorial chemistry [34]. Because of their sensitivity, selectivity and speed, fluorescence assays are key techniques for efficient screening of these compounds. Fast and homogeneous assays, i.e. assays working without a separation step, are made possible by new fluorescence techniqes. Such techniques directly measure changes in physical parameters of fluorescent reference compounds, like rotational or translational diffusion constants, upon release of a fluorescent reference compound from the target in a competitive assay (Fig. 13). In the present paper, we show the feasibility of a homogeneous FCS assay on the well-studied target thrombin.

The biochemical system investigated is shown in Fig. 13. We employed thrombin as a model system to evaluate FCS as an analytical technique for drug screening. Thrombin ($m = 39\,\mathrm{kD}$) is the central protease in the blood coagulation cascade [35, 36]. Thrombin cuts two

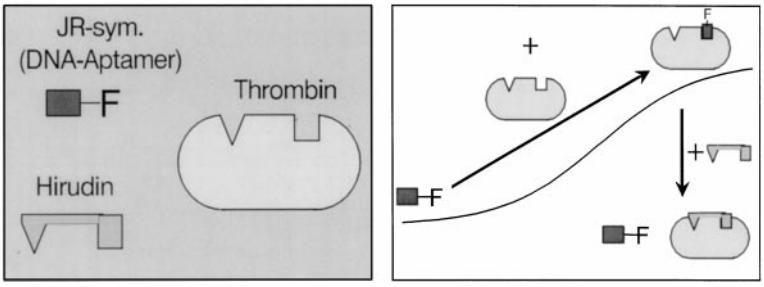

Fig. 13 Competitive assay. The fluorescent labeled JR-sym aptamer, bound to the exosite of thrombin, is displaced by hirudin which simultaneously binds to the active site and exosite. (Left): schematic drawing of thrombin with both its binding sites: active site and the exosite. (Right): experimental procedure, complexation of JR-sym aptamer with thrombin, after the displacement of JR-sym aptamer by the stronger binding hirudin

small peptides from the protein fibrinogen, forming fibrin which in turn polymerizes. To achieve this, thrombin is equipped with two binding sites. The exosite is a positively charged surface area binding fibrinogen and orienting it according to distance and location towards the active site. The active site contains a catalytic pocket of the trypsin type. Two peptide loops restrict the access of proteins to this binding site and are responsible for the high specificity of thrombin.

As thrombin is responsible for the fibrin polymerization and in part for the formation of blood clots in different coagulation-related diseases, it is a well-studied target, and several thrombin inhibitors are known. The inhibitor used in this study was Hirudin, a protein isolated from blood sucking animals. This natural protein is known to bind to both binding sites.

The fluorescent reference compound directed to the exosite (JR-sym.*) is a rhodamine labeled DNA oligomer (for details see [31]).

Reference compound

In a first step of the experiments, the binding of the reference compound to thrombin is observed. Figure 14 shows FCS autocorrelation curves of the free and the bound aptamer JR-sym*. The apparent hydrodynamic diameter calculated by using Eqs. (1) and (2) increases from 3.9 to 7.1 nm after the complex with thrombin has been formed. Figure 15 plots the measured hydrodynamic sizes of the reference compounds vs. the concentration of thrombin. At the starting point and at the end point of the titration curves, the measured hydrodynamic sizes correspond to the size of the free and the bound reference compounds, respectively. The solid line in Fig. 15 is a fit of the data to the model of a two-component complexation in chemical equilibrium. The values for the dissociation constant of the reference compound obtained from the fit were 200 nM.

Competition experiments

We form a complex by incubating a small amount of the reference compound with an excess of thrombin. To this complex, various amounts of thrombin inhibitor is added and the apparent hydrodynamic size of the fluorescent species is monitored with FCS. If the reference compound in the complex with thrombin is replaced by the inhibitor, the hydrodynamic size of the reference compound measured by FCS is reduced. Figure 15 demonstrates the displacement of JR-sym* by hirudin. In analogous experiments, we have investigated the binding of several different thrombin inhibitors to thrombin [31].

This shows, that FCS can be successfully employed to yield quantitative information about biochemical complexation reactions without separation steps.

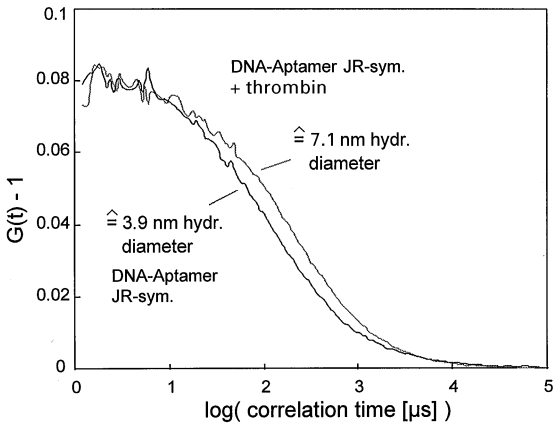

Fig. 14 FCS autocorrelation curves of bound and free DNA-aptamer. An increase in hydrodynamic diameter is found after forming the complex with thrombin

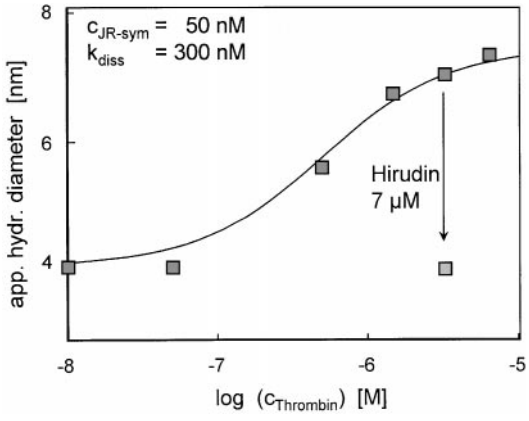

Fig. 15 Competitive assay. The fluorescent labeled JR-sym aptamer, bound to the exosite of thrombin, is displaced by hirudin which simulaneously binds to the active site and exosite. Change of apparent hydrodynamic diameter while following the experimental procedure of Fig. 13

Two-photon fluorescence correlation spectroscopy (TP-FCS) of polymeric lattices

TP-FCS [37] is the extension of FCS using two-photon excitation to confine the measuring volume instead of a confocal aperture. The feasibility of TP-FCS will be demonstrated on Fluorescein labelled latex dispersions (Polysciences) of varying particle sizes. A very simple optical setup of the TP-FCS experiment was used to detect the Fluorescein fluorescence of the latex spheres. A modelocked Ti–sapphire laser emitting pulses of 100 fs duration at a wavelength of 886 nm with a repetition rate of 76 MHz was focused with a 20× microscope objective on a cuvette containing the dispersion. The fluorescence from

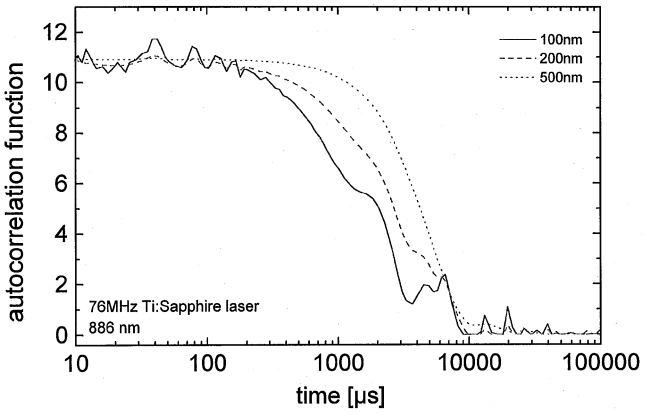

Fig. 16 TP-FCS autocorrelation curves of latex beads with different diameters 100, 200, 500 nm

the focal spot was collected by a lens in rectangular geometry and focused onto a Si avalanche photodiode. To block the laser radiation a short pass filter was placed in front of the detector. The electronic signal of the photodiode was fed into a hardware correlator to record the autocorrelation curves. The very high repetition rate of 76 MHz is quasi-continuous compared to the times scale of the autocorrelation function in Fig. 16 starting at 10 μs. Therefore, no distortion of the correlation function is expected due to the pulsed excitation laser. Figure 16 shows first experimental results. The shape of the correlation curves is affected by laser fluctuations which are to be controlled in future experiments. The measured correlation times are found to be proportional to the particle sizes as predicted by the Stokes–Einstein relationship.

This proves, that TP-FCS can measure the diffusion behaviour of fluorescent particles. The sensitivity is lower than standard FCS and will not reach the single molecule level, but the optical setup can be simpler, it can be parallelized, the combination with time-resolved fluorescence (single-photon counting) is possible in the same experiment and sensitive biological systems will not be photodamaged so easily. This possibly opens the road for direct detection of protein movements via measuring the two-photon- or three-photon-FCS curves of their intrinsic fluorescing amino acids.

Raman correlation spectroscopy to discriminate chemical nature and diffusion

Raman correlation spectroscopy [30] is the vibrational spectroscopic counterpart of FCS. Therefore, it obeys the same fluctuation analysis. In RCS the fluctuations of selected Raman bands are detected instead of fluorescence. Raman scattering suffers from its low scattering cross-section. Therefore, RCS is not a technique to study the diffusion behaviour of single molecules but particles that contain thousands of Raman active molecules. The advantage of RCS is the combination of the chemical identification due to specific Raman bands (intrinsic labeling) with diffusion behaviour due to fluctuation analysis. Informations on particles sizes of different chemical ingredients of liquid formulations can be gained from the analysis of autocorrelation functions of the Raman bands detected. Mixed particle interaction or complexation can be observed by crosscorrelation analysis of signals obtained from particle-specific Raman bands.

The experimental RCS setup, shown in Fig. 17A, is based on a modified confocal Raman microscope. In order to follow fast temporal fluctuations, the CCD-detector of the original microscope is replaced by a linear array of 40 optical fibers (diameter 200 μm, corresponding to a Raman shift of 30 cm^{-1} between adjacent fibers). Two avalanche photodiode detectors can be connected to any two fibers. This, together with the rotation of the grating of the spectrograph, allows to set the detection wavelengths to the desired bands in the Raman spectrum. The signals of the detectors are fed into a hardware correlator, where the autocorrelation functions (ACF) and the crosscorrelation function (CCF) of the observed Raman intensity fluctuations are calculated. The optical setup of RCS is completely analogous to FCS and the resulting ACFs have the same theoretical shape [Eq. (1)].

As an example, we studied the dynamics of β-carotene suspensions of different particle size. The β-carotene suspensions (particle diameter 220 nm according to QELS) were prepared with a micronization technique [39]. Due to its high content of C=C double bonds, β-carotene shows strong Raman scattering with a principal band around 1510 cm^{-1}. Typical Raman intensities observed in our RCS setup are 2–5 kcps (Fig. 17C) at a sample concentration of 0.5–1 wt% carotenoid, with a background intensity of 0.3 kcps. Fitting [background corrected version of Eq. (1)] the ACFs of two different β-carotene suspensions (Fig. 17D, DLS-particle diameters $d_1 = 220$ nm, $d_2 = 150$ nm) yields their characteristic decay times τ and number of particles $N(\tau_1 = 46$ ms, $\tau_2 = 34$ ms, $N_1 = 1.9$, $N_2 = 10.8)$.

With RCS, the dynamic behaviour of one species of particles can be selectively monitored in a mixed particle system, even against a background of a much higher concentration of other particles. This is demonstrated adding a small number (1 : 90 number ratio) of β-carotene particles (DLS diameter 220 nm) to polystyrene (PS) latices (DLS diameter 49 nm, pH 8.5, negligible Raman activity at 1510 cm^{-1}). The ACF of the mixture shows the same dynamics as the ACF of a pure β-carotene sample with twice the β-carotene content (Fig. 18). The ratio of the

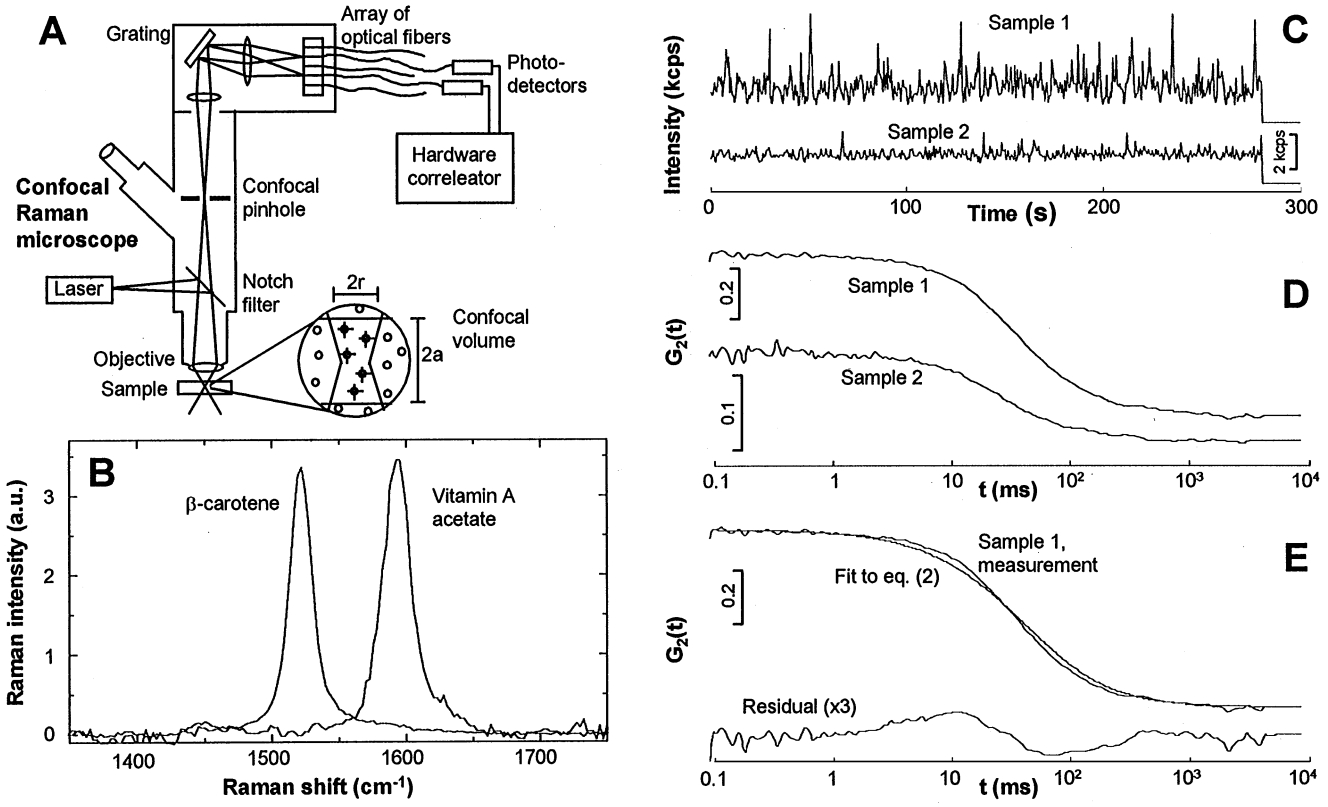

Fig. 17 Overview of the RCS technique. (A) Instrumental setup (B) Raman spectra of the carotenoids of this study (C) Raman intensity traces at 1510 cm^{-1} from two different β-carotene dispersions. Sample 1: particle diameter 220 nm, sample 2: 150 nm, 1 wt% β-carotene in suspension (D) ACFs resulting form the sign intensity traces (E) Comparison of a fit of Eq. (1) to the ACF of sample 1, the residual has been magnified 3× [16]

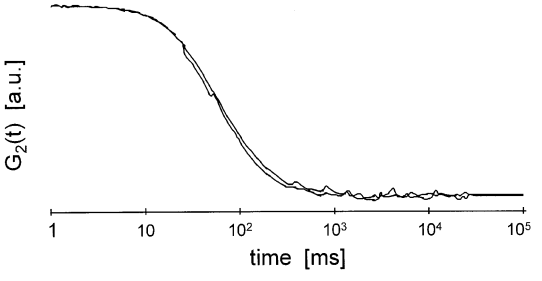

Fig. 18 Autocorrelation curves of pure β-carotene dispersion and a dispersion of β-carotene (200 nm) mixed with polystyrene latices (45 nm) (number ratio 1:90). Due to the Raman detection of the β-carotene C=C-vibration, polystyrene latices do not affect the autocorrelation trace

particle numbers N found in the mixture and in the pure sample is 0.48 [after background correction of Eq. (1), 0.61 without background correction]. This experiment shows that the carotenoid particles can be selectively measured in the mixture and their dynamics are changed only slightly by the presence of the PS latices.

When two detection channels tuned to different Raman shifts are used in the RCS setup, species with different Raman spectra can be observed simultaneously. In addition to their individual dynamics, the simultaneous recording allows the sensitive detection of correlated fluctuations (caused e.g. by complex formation) between the two species via crosscorrelation of the signals.

We studied a 1:3 mixture of β-carotene and vitamin A acetate. With the first detection channel of our RCS setup tuned to 1525 cm^{-1} and the other to 1585 cm^{-1} (two fibers distant in the linear fiber array), the spectra of β-carotene and vitamin A acetate particles can be recorded in the individual channels with little overlap (Fig. 17B). When recording both channels simultaneously, the individual intensities fluctuate independently most of the time, with distinct peaks in the intensity occurring at different times for the individual channels (Fig. 19A). The ACFs of the individual detection channels are identical to the ones seen in pure samples. Sometimes, however, a large signal can be seen in both detection channels exactly simultaneously (Fig. 19B). The CCF of the two detection channels

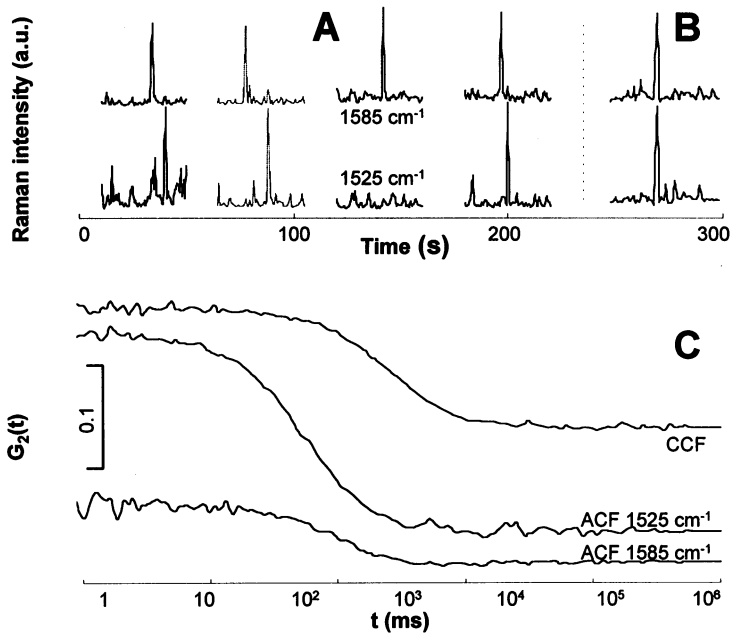

Fig. 19 Dual-channel experiments with mixtures of β-carotene and vitamin A acetate. Channel 1 set to 1525 cm^{-1}, channel 2 to 1585 cm^{-1}. (A) Intensity traces (channel 1 lower, channel 2 upper curves) showing the channels fluctuating independently. (B) Intensity trace showing a simultaneous signal in both channels indicating agglomerates (C) Auto- and crosscorrelation functions from the mixture

shows that the component causing the simultaneous signals in both channels has slower dynamics than the two original carotenoids. (Fig. 19C). This component is likely to be caused by agglomerates β-carotene and vitamin A acetate particles.

The major advantage of RCS over FCS is that RCS can distinguish the components of a colloidal system in their native state without labeling and monitor their dynamic behaviour selectively. We think that with technical improvements in sensitivity, RCS will be a valuable tool in the characterization of complex colloidal systems like coatings, pigments and pharmaceutical formulations.

Summary and outlook

New developments in confocal fluorescence and Raman microscopy lead to an increase in sensitivity, selectivity and speed of microscopic imaging and fluctuation analysis resulting in a better understanding of structure–property relationships essential for targeted development in chemical and pharmaceutical industry.

Raman and fluorescence imaging microscopy can investigate heterogeneous, multiphase solid-state samples according to chemical composition and distribution of sensor molecules exploring local environments due to polarity, aggregation, etc., whereas fluorescence and Raman correlation spectroscopy can be applied to characterize the diffusion behavior of biological and polymeric colloidal systems in the liquid phase. We expect that with a further improved RCS instrumentation, a number of fundamental and applied problems can be addressed using its potential to study dynamics of selected chemical species. For instance, many industrial products like coatings, pigments and pharmaceutical formulations are complex colloidal systems with many open questions on the interactions of the individual components.

Acknowledgements The authors wish to thank T. Friedrich, M. Eustachi, S. Rozouvan, E. Mayer, B. Kren, M. Müller, R. Kaltz and L. Häussling for numerous contributions.

References

1. Amelinckx S, van Dyck D, van Landuyt J, van Tendeloo G (1997) Handbook of Microscopy, Methods I. VCH Verlahgsgesellschaft, Weinheim
2. Lakowicz JR (ed) (1994) Topics in Fluorescence Spectroscopy, Vol 1–4. Plenum Press, New York
3. Wolfbeis O (ed) (1993) Fluorescence Spectroscopy New Methods and Applications. Springer, Berlin
4. Schrader B (1995) Infrared and Raman Spectroscopy. VCH, Weinheim
5. Wilson T, Sheppard C (1984) Theory and Practice of Scanning Optical Microscopy. Academic Press, New York
6. Wilson T (ed) (1984) Confocal Microscopy. Academic Press, London
7. Saleh BEA, Teich MC (1991) Fundamental of Photonics. Wiley, New York
8. Cheo PK (ed) (1989) Handbook of Solid-State Lasers. Optical Engineering, Vol 18. Marcel Dekker, New York

9. Imasaka T (1993) Semiconductor Laser Spectrometry. Anal Sci 9:329–344
10. Shen YR (1984) The Principles of Nonlinear Optics. Wiley, New York
11. Neumann E-G (1988) Single Mode Fibers. Springer, Berlin
12. Tedesco JM, Owen H, Pallister DM, Morris MD (1993) Anal Chem 65: 441A
13. Williams KPJ, Batchelder DN (1994) Spectroscopy Europe 6:19
14. Dautet H, Deschamps P, Dion B, MacGregor AD, MacSween D, Mclntyre RJ, Trottier C, Webb PP (1993) Photon counting techniques with silicon avalanche photodiodes. Appl Opt 32: 3894–3900
15. Birch JS, Hungerford G (1994) Instrumentation for Red/Near-Infrared Fluorescence. In: Lakowicz JR (ed) Topics in Fluorescence Spectroscopy. Plenum Press, New York, pp 377–416
16. Denk W, Piston DA, Webb WW (1995) Two-photon molecular excitation in laser-scanning microscopy. In: Pawley JP (ed) Handbook of Biological Confocal Microscopy. Plenum Press, New York
17. Schlarb B, Heckmann W, Schwarzenbach E, submitted for publication in Colloid and Interface Science
18. Brulé B, Brion Y, Tanguy A (1988) Asphalt Paving Technol 57:42
19. Markwort L, Kip B, Da Silva E, Roussel B (1995) Appl Spectrosc 49: 1411–30
20. Williams KPJ, Pitt GD, Batchelder DN, Kip BJ (1995) Confocal Raman Microscopy Using a Stimatic Spectrograph and CCD Detector. Appl Spectrosc 48:232–5
21. Claybourn M, Luget A, Williams KPJ (1995) Raman Microscopy and Imaging of Polymers. In: Urban MW, Provder T (eds) Multidimensional Spectroscopy of Polymers. ACS Symp Ser 598: 41–60
22. Fouassier JP (1995) Photoinitiation, Photopolymerization and Photocuring. Hanser Publishers, München
23. Pappas SP (ed) (1992) Radiation Curing, Science and Technology. Plenum Press, New York
24. Decker C, Moussa K (1990) J Coat Technol 62:55–61
25. Schrof W, Haeussling L (1997) Tiefenauflösung der Trocknungsvorgänge in Lackfilmen. Farbe & Lack 103: 22–27
26. Buist JM, Grayson SJ, Woolley WD (eds) (1987) Fire and Cellular Polymers. Elsevier Applied Science, Amsterdam
27. Magde D, Elson E, Webb W (1972) Phys Rev Lett 29:705
28. Rigler R, Widengren J, Mets U (1993) In: Wolfbeis O (ed) Fluorescence Spectroscopy. Springer, Berlin, pp 13–24
29. Thompson NL (1991) Fluorescence correlation spectroscopy. In: Lakowicz JR (ed) Topics in Fluorescence Spectroscopy, Vol 1: Techniques. Plenum Press, New York
30. Schrof W, Klingler J, Rozouvan S, Horn D (1998) Raman correlation spectroscopy: a new method for studying chemical composition and dynamics of disperse systems, Phys Rev E 57:R2523-6
31. Klingler J, Friedrich T (1997) Site specific Interaction of Thrombin and Inhibitors observed by Fluorescence Correlation Spectroscopy. Biophys J 73: 2195–2200
32. Rigler RJ (1995) Biotechnology 41:177
33. Horn D, Klingler J, Schrof W, Graf K. Experimental Progress in the Characterization of Colloidal Systems. Progress Coll & Polym Science, in print
34. Campbell P (ed) Intelligent drug design. Nature 384:(1996) (suppl.) issue no. 6604 (7 Nov 1996)
35. Jackson CM (1980) Blood coagulation. Annual Reviews in Biochemistry 49: 765–811
36. Davie EW, Fujikawa K, Kisiel W (1991) The coagulation cascade: initiation, maintainance and regulation. Biochemistry 30:10363–10370
37. Berland KM, So PTC, Graton E (1995) Two-Photon Fluorescence Correlation Spectroscopy: Method and Application to the Intracellular Environment. Biophys J 68:694–701
38. The straight part at the end of the intensity traces and ACFs indicates the respective baseline, i.e. 0 cps for the intensity traces and 1.0 for the ACFs
39. Wiese H, Horn D (1993) Ber Bunsenges. Phys Chem 97:1589